

Stepwise Recruitment of Transcellular and Paracellular Pathways Underlies

Blood-Brain Barrier Breakdown in Stroke

Daniel Knowland^{1,8}, Ahmet Arac^{2,3,8}, Kohei Sekiguchi^{4,5}, Martin Hsu¹, Sarah E. Lutz¹,
John Perrino⁶, Gary K. Steinberg², Ben A. Barres⁷, Axel Nimmerjahn^{4,9,10} and Dritan Agalliu^{1,9,10}

1. Department of Developmental and Cell Biology, University of California, Irvine, CA
92697
2. Department of Neurosurgery, Stanford University School of Medicine, Stanford, CA 94305
3. Department of Medicine, University of California at Irvine, Orange, CA 92868
4. Waitt Advanced Biophotonics Center, The Salk Institute for Biological Sciences, La Jolla,
CA 92037
5. Biological Sciences Graduate Program, University of California, San Diego, La Jolla, CA
92037
6. Electron Microscopy Facility, Stanford University School of Medicine, Stanford, CA
94305
7. Department of Neurobiology, Stanford University School of Medicine, Stanford, CA 94305
8. These first authors contributed equally to this work
9. These senior authors contributed equally to this work
10. Correspondence: dagalliu@uci.edu and animmerj@salk.edu

Supplemental Information

Supplemental Figures and Legends

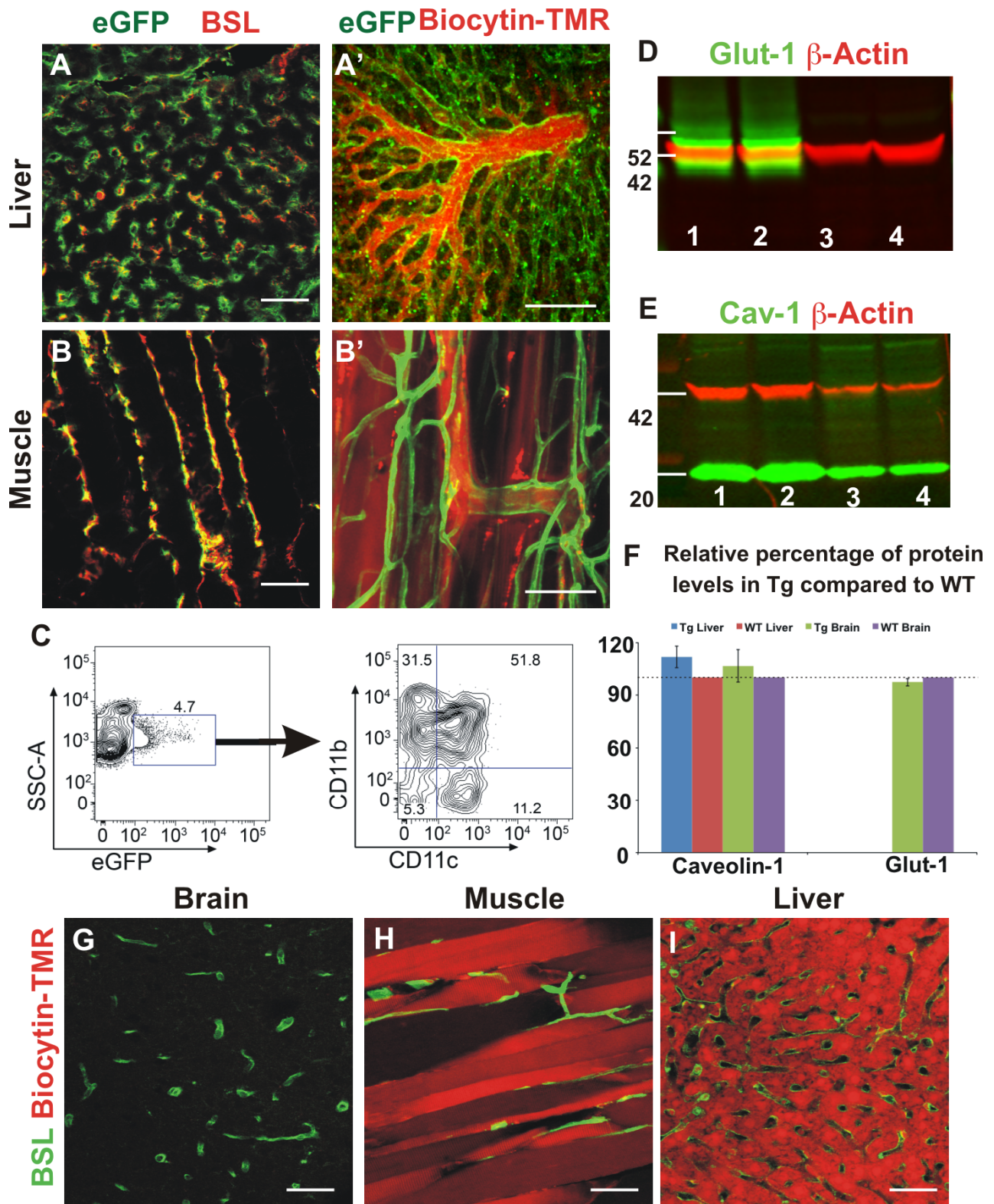


Figure S1. Characterization of eGFP expression in liver and muscle endothelium and BBB structure and function in healthy *Tg eGFP-Claudin5* animals, related to Figure 1. (A,B) Expression of eGFP-Claudin5 fusion protein in liver (A) and muscle (B) blood vessels labeled with *Griffonia (Bandeiraea) simplicifolia* Lectin I (BSL I). (A',B') Maximum intensity projections of 80 μm and 250 μm thick surface tissue volumes from liver (A') and muscle (B') recorded with two-photon microscopy in anesthetized *Tg eGFP-Claudin5* mice. Biotin-TMR (1%) was injected into the tail vein to visualize blood plasma and determine vascular permeability. The tracer leaks out from the blood vessels into the liver and muscle in healthy mice. Note that the eGFP-Claudin5 fusion protein is not localized to TJs in liver or muscle endothelial cells. (C) Flow cytometry plot showing the fraction of eGFP⁺ cells in blood that are CD45⁺ (SSC-A) (left panel) and the proportions of myeloid (CD11b⁺) and lymphoid (CD11c⁺) populations (right panel; see also Table S1). (D,E) Western blots from brain (lanes 1, 2) and liver (lanes 3, 4) lysates of *Tg eGFP-Claudin5* (lanes 1, 3) and wild-type mice (lanes 2, 4), for Glut-1 (52 kDa) and β -actin (42 kDa) (D) or Caveolin-1 (20 kDa) and β -actin (E). (F) Quantitation of Caveolin-1 and Glut-1 relative protein levels in brain or liver of *Tg eGFP-Claudin5* and wild-type mice. Caveolin-1 and Glut-1 levels in wild-type mice were used as standards. Caveolin-1 and Glut-1 protein levels in transgenic mice are presented as a percentage of the respective protein levels in wild-type mice, with each being normalized to its respective β -actin control values. There is no significant change in the amount of Caveolin-1 protein in liver or brain endothelial cells from transgenic mice. (G-I) Analysis of biotin-TMR tracer leakage 30 min after tracer injection in healthy brain (G), muscle (H) or liver (I) from *Tg eGFP-Claudin5* mice. The biotin-TMR leaks out from muscle and liver, but not brain, blood vessels labeled with BSL-I in transgenic mice. Scale bars = 100 μm (A',B'); 50 μm (A,B,G-I).

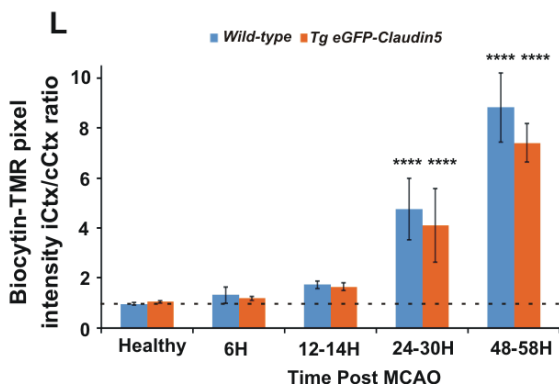
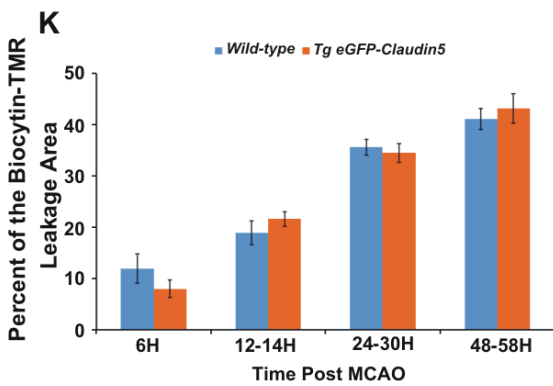
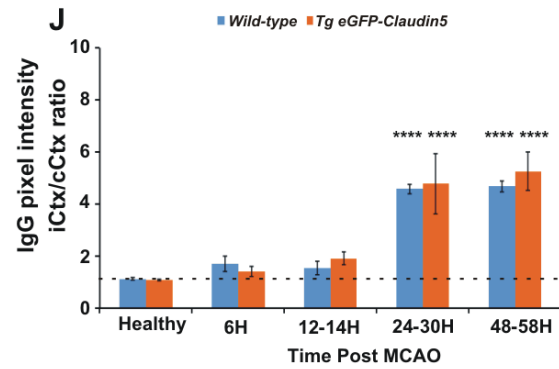
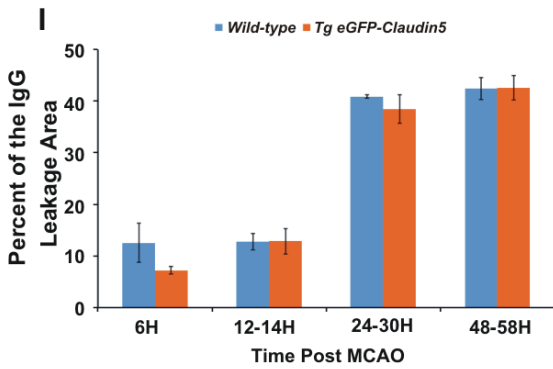
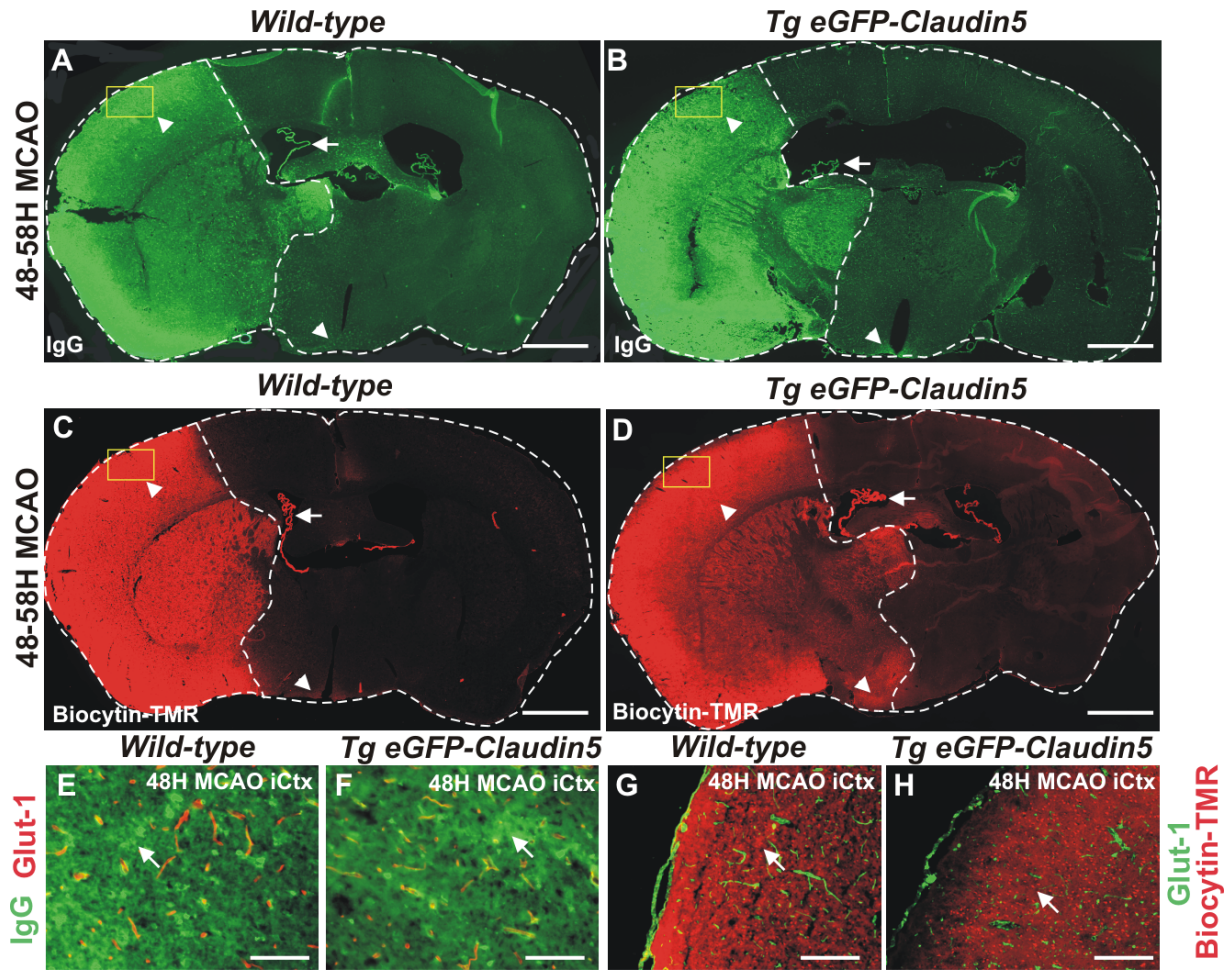


Figure S2. *Tg eGFP-Claudin5* mice display increased IgG and paracellular biocytin-TMR leakage during stroke progression that is similar to wild-type mice, related to Figure 2. (A-D) IgG and Biocytin-TMR leakage in brain sections from wild-type (A,C) and *Tg eGFP-Claudin5* mice (B,D) 48-58 h post-t-MCAO. Dashed white lines mark the areas of IgG or biocytin-TMR leakage within the brain and tissue borders. The choroid plexus is intensely labeled with IgG and biocytin-TMR on both ipsilateral and contralateral sides, due to absence of the BBB (white arrows). (E-H) Higher magnification images for the yellow squares shown in (A-D) within the 48 h post-t-MCAO cortex in wild-type (E,G, respectively) or *Tg eGFP-Claudin5* (F,H, respectively) mice. The IgG or biocytin-TMR tracer leaks out of the Glut-1⁺ blood vessels into the CNS parenchyma (white arrows). (I-K) Bar graph of the fraction of IgG (I) or biocytin-TMR leakage area (K) in wild-type or *Tg eGFP-Claudin5* mice. The increase in either IgG or biocytin-TMR leakage area fraction during disease progression is similar between wild-type and transgenic mice. (J,L) Bar graphs showing IgG (J) or biocytin-TMR (L) average pixel intensity ratios between ipsilateral and contralateral cortices in wild-type (blue bars) and *Tg eGFP-Claudin5* mice (orange bars) with t-MCAO. There is no significant difference in biocytin-TMR leakage average pixel intensity between wild-type and transgenic mice at any given time point. Data in Figures S2I-L were collected from 9-35 independent fields of view that contained cortical venules or capillaries from wild-type or *Tg eGFP-Claudin5* mice (n = 3-5 mice per time point). Data are represented as mean ± s.e.m, ****p<0.0001. Scale bars = 400 μm (A-D) and 50 μm (E-H).

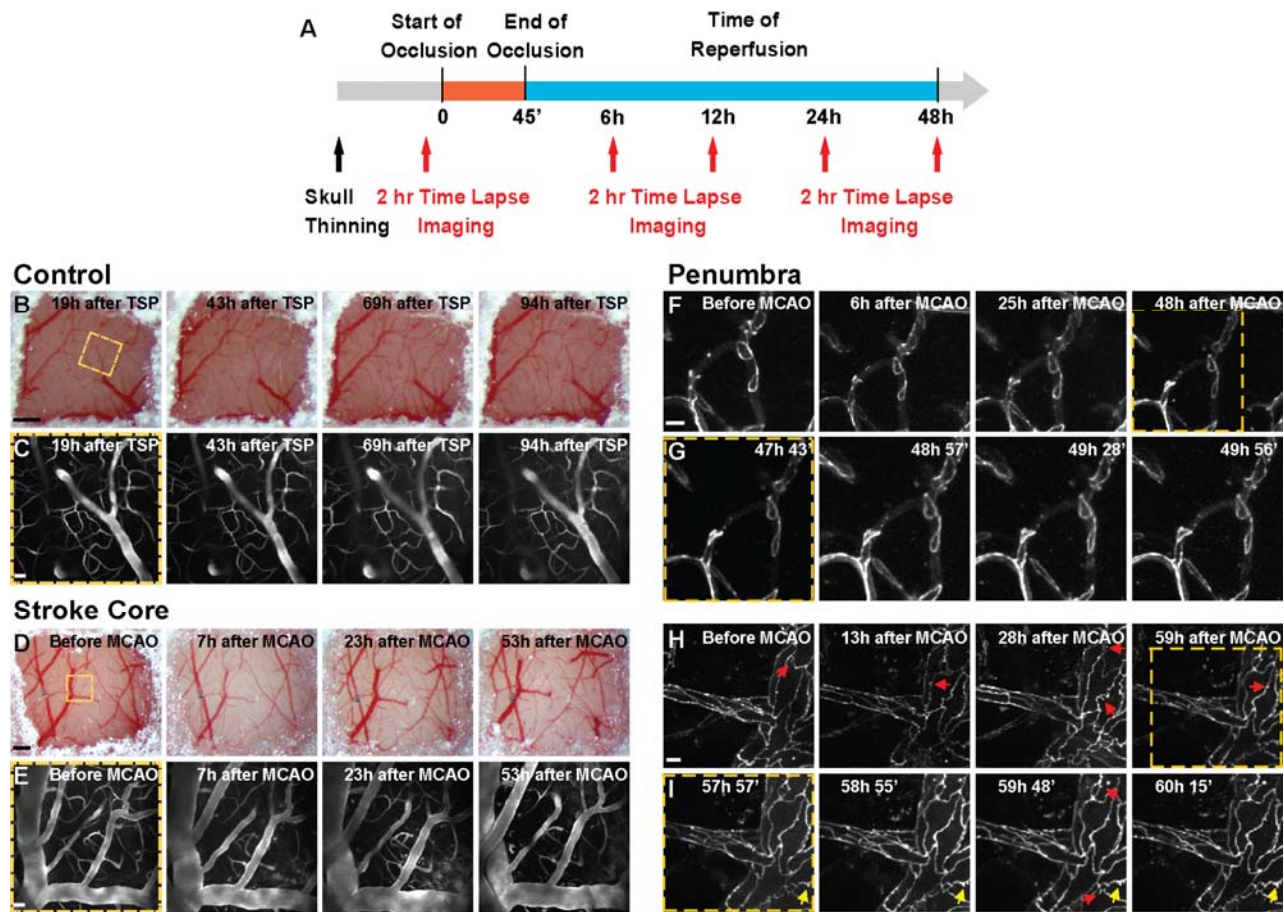


Figure S3. Continual two-photon time-lapse imaging of cortical blood vessels and tight junctions within the cortical penumbra region in *Tg eGFP-Claudin5* mice, related to Figure 3. (A) Diagram of the experimental procedure for continuous, transcranial two-photon time-lapse imaging of *Tg eGFP-Claudin5* mice. Four imaging sessions were conducted in both control and stroke animals. Each session lasted ~2 h and involved repeated optical recordings (every 15-25 min) from distinct cortical volumes. Stroke animals were imaged once before and at three time points after t-MCAO (~6h or 12h, ~24h and 48h). Control animals were imaged at corresponding time points. Imaging began ~24 h after thinned skull preparation (TSP). (B,D) Digital camera images of surface (dura and cortical) blood vessels below the TSP from a control (B; 19-94 h after TSP) or stroke (D; before and 7-53 h after t-MCAO) animal. Camera images were taken just prior

to each imaging session. Note that the surface blood vessel pattern remains stable in control mice but cortical vessels shift relative to dura vessels in stroke mice, likely due to tissue edema. Additionally, some cortical blood vessels undergo progressive rearrangements following t-MCAO. (C,E) Maximum intensity projection images of cortical blood vessels within 145 and 150 μm thick volumes recorded with two-photon microscopy from the yellow-boxed area shown in B and D, for the control or stroke animal, respectively. Tail vein injection of biocytin-TMR (1% in PBS) was used to visualize blood plasma and determine vascular permeability. (F-I) Time-lapse images of eGFP-positive TJs in capillaries (F,G) and venules (H,I) from the penumbra region, defined *post hoc* 48-60 h post t-MCAO by the amount of tracer (biocytin-TMR) leakage in the parenchyma (data not shown). Images in F and H are from different days/imaging sessions. Images in G and I are from a selected day/imaging session (indicated by the yellow boxed region in F and H). Note that there are many protrusions in venules but not capillaries. Static protrusions present in all images (H,I) during the time lapse are labeled with a yellow arrow, dynamic protrusions are labeled with red arrows. Protrusions are particularly dynamic in venules during the 57-60 h period after t-MCAO. See also Movies S7-S8. Scale bars = 0.25 mm (B,D), 25 μm (C,E) and 10 μm (F-I).

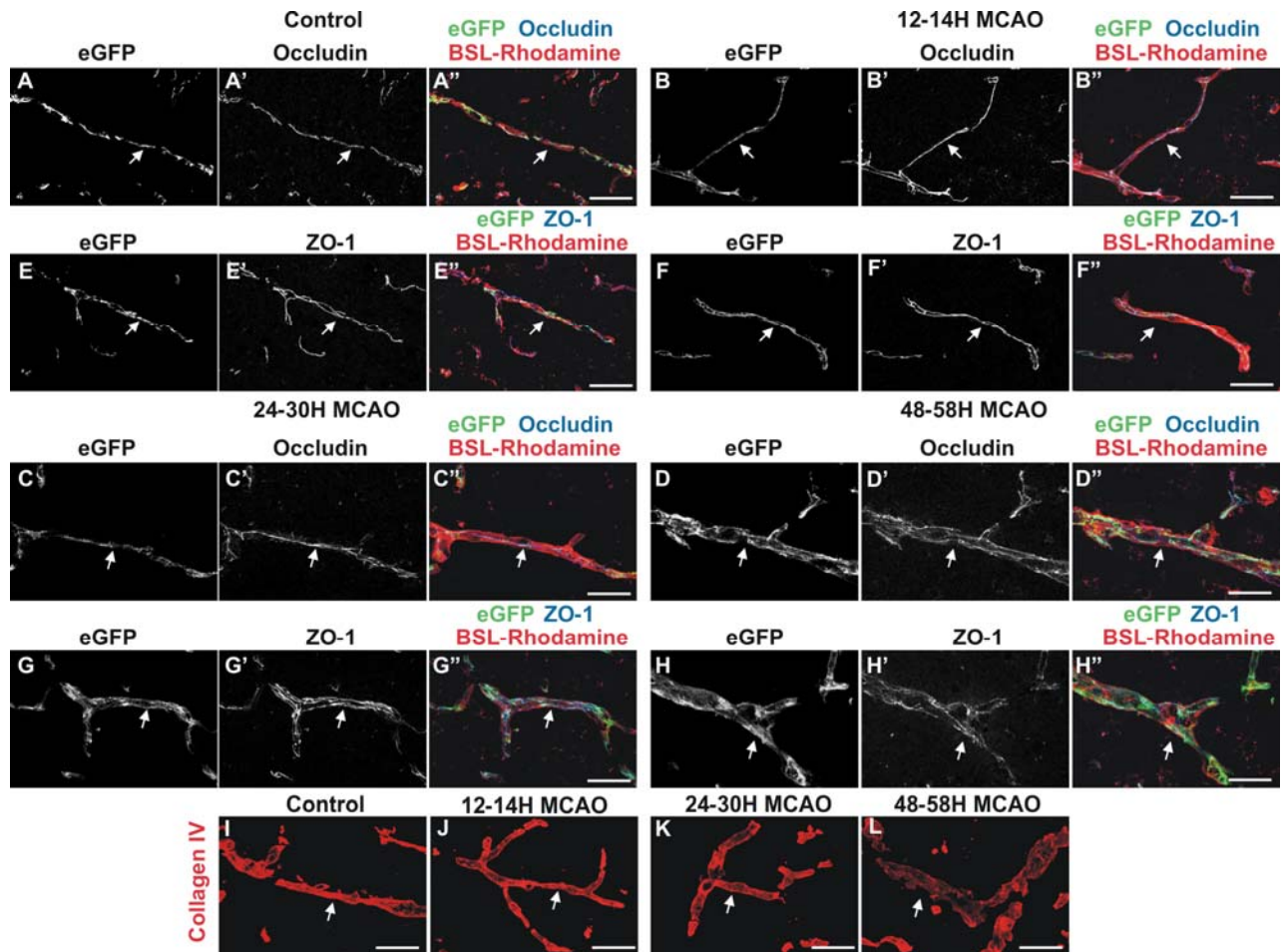


Figure S4. Changes in tight junction and basement membrane protein expression during stroke progression in *Tg eGFP-Claudin5* mice, related to Figure 4. (A-H'') Expression of eGFP (A-D), Occludin (A'-D') and BSL-rhodamine (A''-D'') or eGFP (E-H), ZO-1 (E'-H') and BSL-rhodamine (E''-H'') in TJs of cortical blood vessels from either healthy or t-MCAO-subjected *Tg eGFP-Claudin5* mice. eGFP localizes to TJ strands together with Occludin and ZO-1 in healthy animals, at 12-14 h post-t-MCAO or in most cortical blood vessels at 24-30 h post-t-MCAO. However, at 48-58 h post-t-MCAO eGFP is distributed both at TJs and within endothelial cells labeled with BSL-rhodamine (D-D'', H-H''; white arrows). In addition, there is a cellular mislocalization and reduction in Occludin and ZO-1 levels (D-D'', H-H''; white arrows).

Expression of endothelial basement membrane protein Collagen IV (I-L) in cortical blood vessels from healthy *Tg eGFP-Claudin5* mice or after t-MCAO (stroke core region). The levels of Collagen IV are reduced 48-58 h post-t-MCAO (L). Scale bars = 50 μ m.

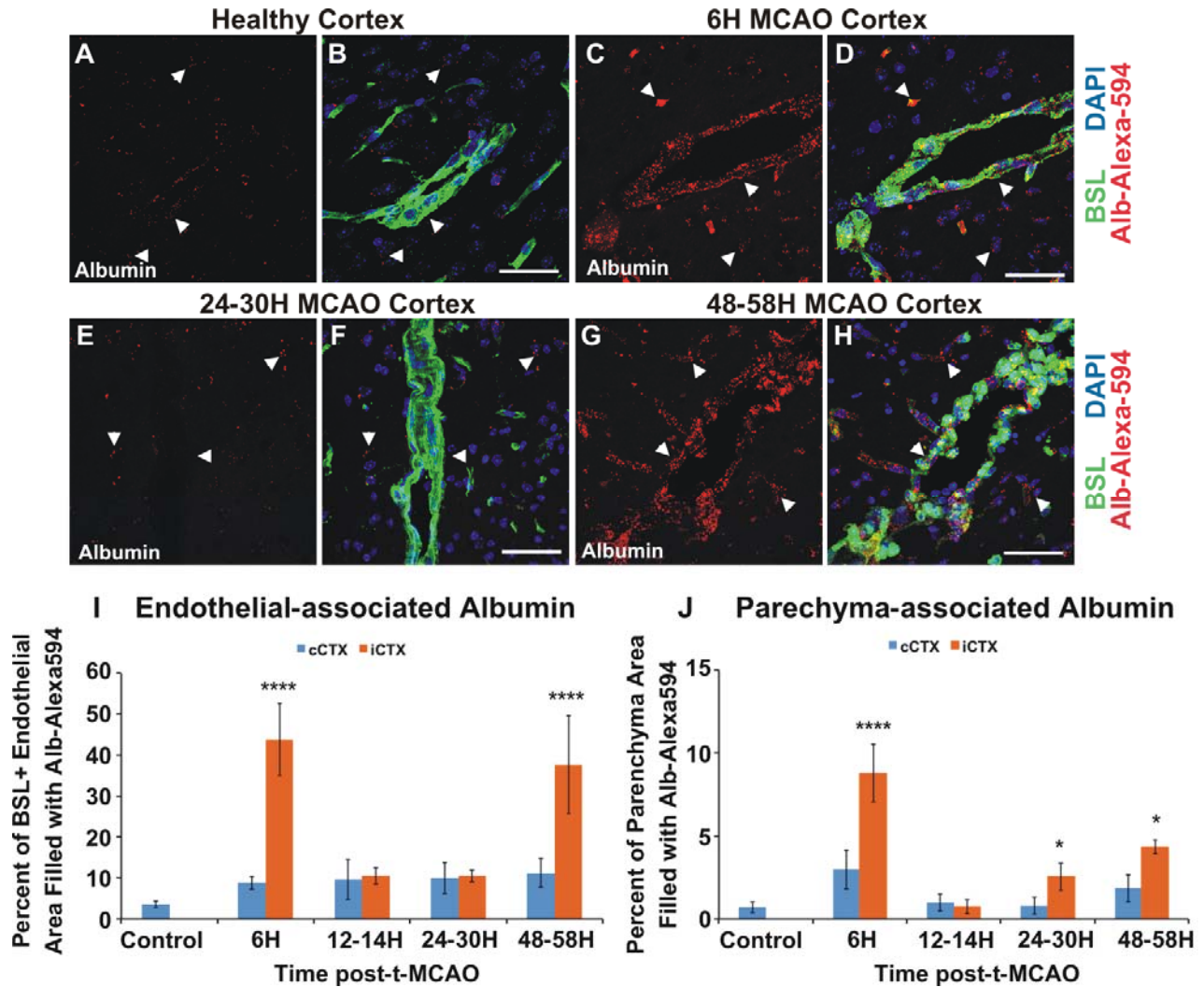


Figure S5. CNS endothelial endocytosis and transcytosis are upregulated as early as 6 h following stroke, related to Figure 6. (A-H) Uptake of alb-Alexa594 in healthy cortex (A,B) and ipsilateral stroke cortex 6 h, 24-30 h and 48-58 h post-t-MCAO (C-H). Note the increase in alb-Alexa594 uptake within CNS endothelium labeled with BSL in merged panels, as early as 6 h

post-t-MCAO (white arrowheads). (I,J) Bar graphs showing the fraction of BSL⁺ endothelial (I) or brain parenchyma (J) area filled with alb-Alexa594 in ipsilateral (orange) and contralateral (blue) cortex. The percentage of endothelial and parenchyma-filled area with alb-Alexa594 is significantly higher 6 h and 48 h post-t-MCAO as compared to healthy cortex. The data were collected from 4-9 independent fields of view that contained cortical venules or capillaries (n = 3-5 animals per time point). Data are represented as mean ± s.e.m, *p<0.05; ****p<0.0001, mixed effect ANOVA. Scale bars = 50 μm.

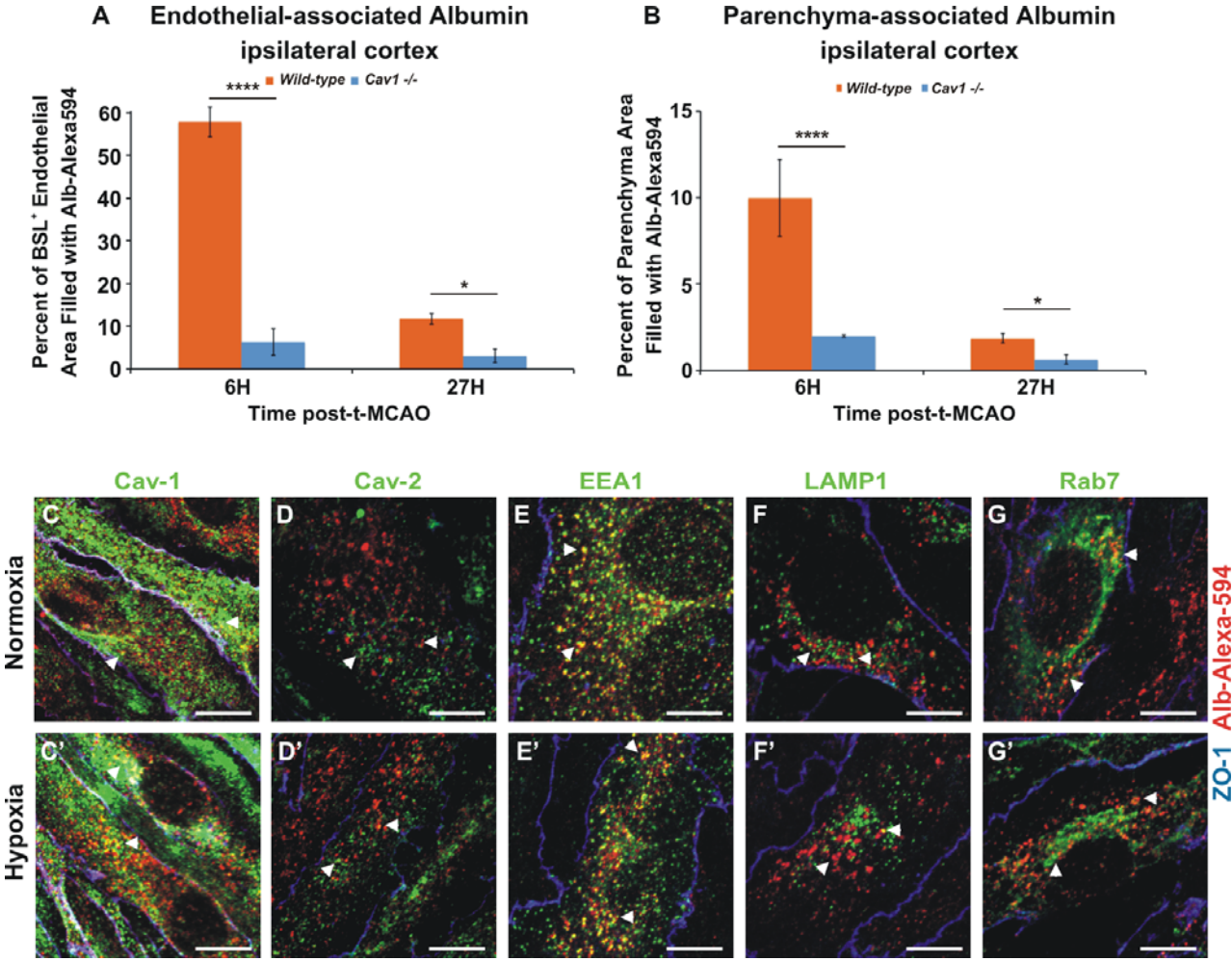


Figure S6. The reduction in albumin endocytosis and transcytosis in *Cav1*-deficient CNS endothelium is due to the presence of albumin within the endosomal compartment, related to

Figure 7. (A,B) Bar graphs showing the percent of BSL⁺ endothelial (A) or brain parenchyma (B) area filled with alb-Alexa594 in the ipsilateral cortex of wild-type (orange) or *Cav1*^{-/-} mice (blue) 6 and 27 h post-t-MCAO. The percentage of endothelium- and parenchyma-filled area with alb-Alexa594 is significantly reduced both at 6 h and 27 h post-t-MCAO in *Cav1*^{-/-} mice compared to controls. Data were collected from 4-9 independent fields of view that contained cortical venules or capillaries (n = 3 animals per time point; data are represented as mean ± s.e.m, *p<0.05; ****p<0.0001, mixed effect ANOVA). (C-G') Primary brain endothelial cells (BECs) isolated from P2 cortices and cultured under normoxic or hypoxic conditions were incubated with alb-Alexa594 (red in all images). Alb-Alexa594 colocalizes with Caveolin-1 (C,C') but not Caveolin-2 (D,D'), the lysosome marker LAMP1 (F,F') or the late endosome marker Rab7 (G,G') under normal or hypoxic conditions. However, some alb-Alexa594 is present within early EEA-1⁺ endosomes (E) of primary BECs cultured under normoxic conditions. The amount of alb-Alexa594 is increased in the early endosomes after hypoxia (E', white arrowheads). ZO-1 (blue) marks TJs between endothelial cells in all merged panels. Scale bars = 25 μm.

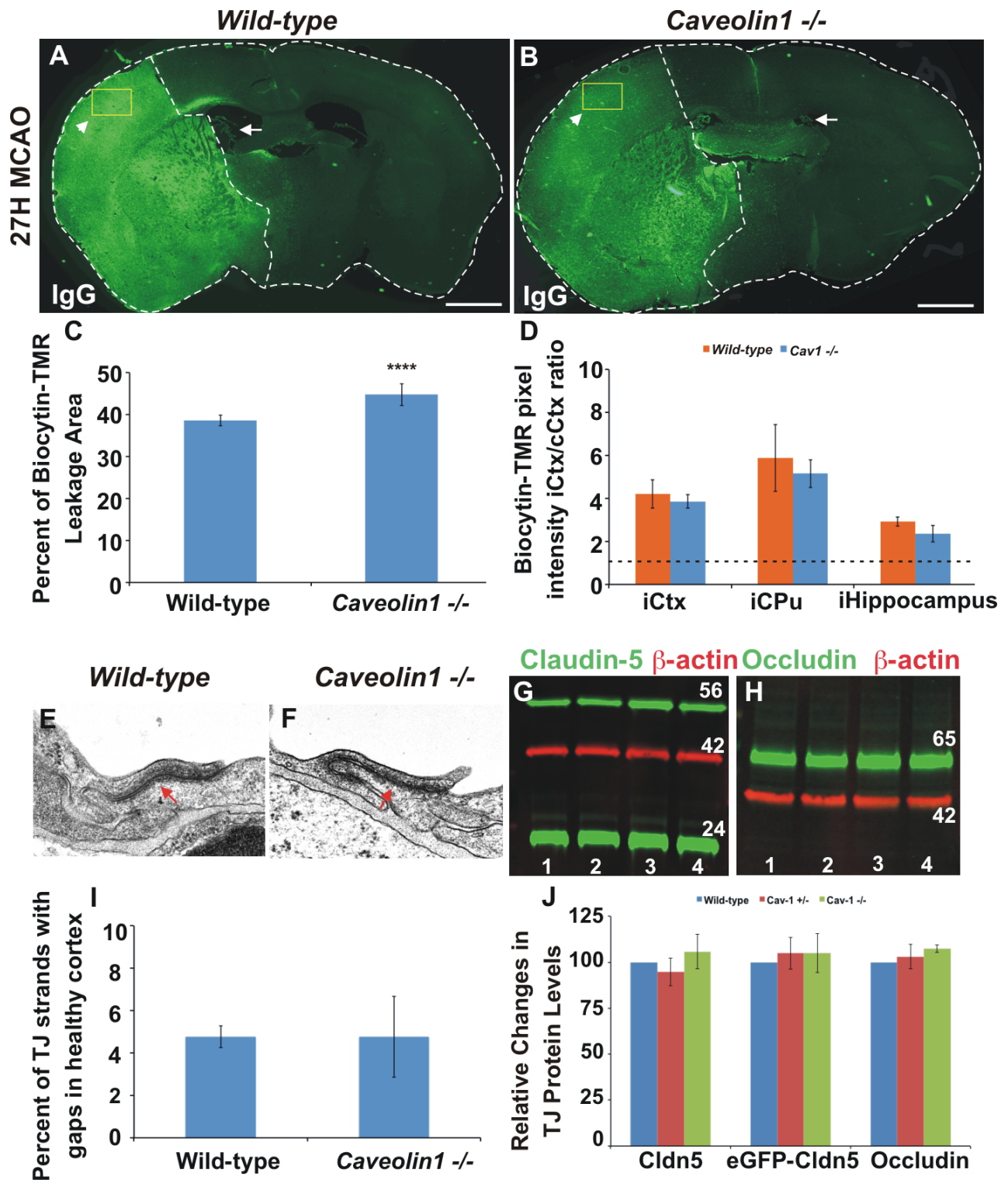


Figure S7. *Cav1*-deficient mice display increased IgG leakage following t-MCAO that is similar to wild-type mice, related to Figure 8. (A, B) IgG leakage in brain sections from wild-

type (A) or *Cav1*^{-/-} (B) mice at 27 h post-t-MCAO. The area of IgG leakage and the outline of the brain are marked with dashed white lines. The choroid plexus (A, B; arrows) is intensely labeled on both ipsilateral and contralateral sides, due to the absence of the BBB. (C) Bar graph showing the percent of IgG leakage area in wild-type or *Cav1*^{-/-} mice. The increased fraction of IgG leakage areas in mutant mice is due to the presence of IgG in the thalamus. (D) Bar graph of the IgG average pixel intensity ratio between ipsilateral and contralateral areas for cortex, putamen and hippocampus in wild-type (orange bars) or *Cav1*^{-/-} mice (blue bars). There is no significant difference in IgG leakage intensity between wild-type and *Cav1*^{-/-} mice in matched anatomical regions. (E, F) TEM images of cortical TJs from healthy wild-type (E) or *Cav1*^{-/-} (F) mice. *Cav1*^{-/-} mice have normal TJ morphology by TEM (red arrow). (G, H) Western blots from brain lysates of *Tg eGFP-Claudin5* (lanes 1 & 2) and *Tg eGFP-Claudin5 Cav1*^{-/-} mice (lanes 3 & 4) for Claudin-5, Occludin (65 kDa) and β -actin (42 kDa). The fusion protein is 56 kDa and endogenous Claudin5 is 24 kDa. (I) Bar graph showing the fraction of TJ strands with gaps, in healthy cortex from *Tg eGFP-Claudin5* and *Tg eGFP-Claudin5 Cav1*^{-/-} mice. There is no difference between the two strains. Data were accumulated from 70 independent fields of view (2.6 μ m X 1.7 μ m) that contained between 1-4 ECs from venules or capillaries in healthy cortex (n = 2 transgenic animals). (J) Bar graph of relative differences in eGFP-Claudin5 fusion protein levels compared to endogenous Claudin5 and Occludin protein levels in *Tg eGFP-Claudin5* versus *Tg eGFP-Claudin5 Cav1*^{-/-} mice. Levels of endogenous Claudin5 and Occludin were used as standards. There is an equal amount of eGFP-Claudin5 and endogenous Claudin5 protein in brains from various mouse strains. Data are represented as mean \pm s.e.m, ****p<0.0001, paired t-test, n = 3 animals per each graph. Scale bars = 400 μ m (A-B).

Table S1. Expression profile of GFP⁺ immune cells in *Tg eGFP-Claudin5* mice, related to Figure S1. A small percentage (~6%) of immune cells in various immune tissues are GFP-positive. CD3⁺, CD4⁺ and CD8⁺ T cells are GFP-negative (n = 3 animals). Data are presented as mean ± s.e.m.

	GFP ⁺ cell percentage among CD45 ⁺ cells	Percentage of cell types among CD45 ⁺ GFP ⁺ cells			
		CD11c ⁺ CD11b ⁺ (myeloid dendritic cells)	CD11c ⁺ CD11b ⁻ (lymphoid dendritic cells)	CD11c ⁻ CD11b ⁺ (other myeloid cells)	B220 ⁺ cells (B cells and some myeloid cells)
Blood	4.6±0.06	52.9±0.5	8.9±1.8	30.9±0.8	9.4±0.7
Bone marrow	5.6±0.04	11.9±0.3	17.5±1.8	40.9±0.4	39.1±1.5
Lymph node	0.6±0.06	45.3±3.9	12.6±3.3	15.8±2.1	24.4±2.5
Spleen	2.7±0.23	54±0.5	22.6±0.9	13.7±0.8	20.9±2.6

Movie S1: Visualization of BBB structural and functional integrity in healthy mouse cortex, related to Figure 1. Z-stack of two-photon images recorded in the cortex of an anesthetized healthy *Tg eGFP-Claudin5* mouse. The depth of recording below the pial surface is indicated in the upper right corner. eGFP-labeled TJs between endothelial cells in arteries, arterioles, venules and capillaries are shown in green. Tail vein injection of biocytin-TMR was used to visualize cortical blood vessels (red) and assess BBB functional integrity. Note that the biocytin-TMR tracer

is still contained within blood vessels 1 h after intravenous dye injection, indicating that TJs are intact. Scale bar = 25 μm .

Movie S2. Visualization of structural and functional BBB integrity in the ipsilateral stroke cortex 24 hours post-t-MCAO, related to Figure 2. Z-stack of two-photon images showing a 100 μm -thick cortical volume recorded in an anesthetized *Tg eGFP-Claudin5* mouse 24 h post-t-MCAO. Recording depth below the pial surface is indicated in the upper right corner. eGFP-labeled tight junctions between endothelial cells in venules and capillaries are shown in green. Tail vein injection of biocytin-TMR was used to visualize cortical blood vessels and determine BBB functional integrity. Note that <30 min after intravenous injection, the biocytin-TMR tracer has leaked from the blood vessels into the CNS parenchyma. Nevertheless, eGFP-positive TJ strands appear mostly intact and uniform at this time after stroke. Black shadows surrounding cortical capillaries presumably represent swollen astrocyte end feet. Scale bar = 25 μm .

Movie S3. Continual two-photon time-lapse imaging of tight junctions in healthy cortical capillaries, related to Figure 3. Two-photon time-lapse recordings from an anesthetized healthy *Tg eGFP-Claudin5* mouse showing maximum intensity projection images of the same 70 μm -thick cortical volume (sampled with 1 μm axial step size) from four different two-hour imaging sessions after thinned skull preparation (TSP). Elapsed time after TSP is indicated in upper right corners. eGFP-labeled TJs (white strands) show no observable structural changes during the recording period. Scale bar = 10 μm .

Movie S4. Continual two-photon time-lapse imaging of tight junctions in healthy cortical venules, related to Figure 3. Two-photon time-lapse recordings from an anesthetized healthy *Tg eGFP-Claudin5* mouse showing maximum intensity projection images of the same 100 μm -thick cortical volume (sampled with 1 μm axial step size) from four different two-hour imaging sessions after thinned skull preparation (TSP). Elapsed time after TSP is indicated in upper right corners. eGFP-labeled TJs (white strands) in venules have more protrusions than capillaries (see Figure 2N,O). While these protrusions were quite static during two-hour imaging sessions they showed some morphological alterations across days/imaging sessions. Scale bar = 10 μm .

Movie S5. Continual two-photon time-lapse imaging of tight junctions in cortical capillaries within the stroke core region, related to Figure 3. Two-photon time-lapse recordings from an anesthetized *Tg eGFP-Claudin5* mouse showing maximum intensity projection images of the same 100 μm -thick cortical volume (sampled with 1 μm axial step size) from one two-hour imaging session before and three different two-hour imaging sessions after t-MCAO. Elapsed times with respect to reperfusion onset following a 45 min t-MCAO are indicated in upper right corners. Note the progressive change in TJ structure (white strands) and the rearrangement of some blood vessels after stroke. Scale bar = 10 μm .

Movie S6. Continual two-photon time-lapse imaging of tight junctions in cortical venules within the stroke core region, related to Figure 3. Two-photon time-lapse recordings from an anesthetized *Tg eGFP-Claudin5* mouse showing maximum intensity projection images of the same 100 μm -thick cortical volume (sampled with 1 μm axial step size) from one two-hour imaging session before and three different two-hour imaging sessions after t-MCAO. Elapsed times with

respect to reperfusion onset following a 45 min t-MCAO are indicated in upper right corners. Note the progressive change in eGFP-labeled TJ (white strands) structure and dynamics after stroke, particularly during the 53-55 h recording period post-t-MCAO. Scale bar = 10 μ m.

Movie S7. Continual two-photon time-lapse imaging of tight junctions in cortical capillaries within the penumbra region, related to Figure S3. Two-photon time-lapse recordings from an anesthetized *Tg eGFP-Claudin5* mouse showing maximum intensity projection images of the same 70 μ m thick cortical volume (sampled with 1 μ m axial step size) from one two-hour imaging session before and three different two-hour imaging sessions after t-MCAO. Elapsed time with respect to reperfusion onset following a 45 min t-MCAO is indicated in upper right corners. eGFP-labeled TJs (white strands) do not show any major structural changes during and over the four imaging sessions. Scale bars = 10 μ m.

Movie S8. Continual two-photon time-lapse imaging of tight junctions in cortical venules within the penumbra region, related to Figure S3. Two-photon time-lapse recordings from an anesthetized *Tg eGFP-Claudin5* mouse showing maximum intensity projection images of the same 100 μ m-thick cortical volume (sampled with 1 μ m axial step size) from one two-hour imaging session before and three different two-hour imaging sessions after t-MCAO. Elapsed time with respect to reperfusion onset following a 45 min t-MCAO is indicated in upper right corners. Note the progressive change in eGFP-labeled TJ (white strands) structure and dynamics after stroke, particularly during the 58-60 h recording period post-t-MCAO. Scale bar = 10 μ m.

Supplementary Experimental Procedures

Generation of *Tg eGFP-Claudin-5* transgenic mice. A full-length mouse Claudin5 cDNA was inserted into the eGFP-C1 vector (Clontech Inc., Mountain View, CA). The fusion of eGFP with the N-terminus of Claudin-5 (eGFP-Claudin5) cDNA was digested with *NheI/EcoRI* and subcloned into the pCAGGS vector. The eGFP-Claudin-5-rabbit β -globin polyA signal was subcloned into pBS containing the 2.5 kb promoter of the murine *Tie2/Tek1* gene (Evans et al., 2000; Schlaeger et al., 1997). Finally, the 10kb *Tie2/Tek1* enhancer containing exon 1 was inserted downstream of the rabbit β -globin polyA sequence. The entire construct was digested from the pBS backbone with *SaII* and *NotI* and injected into mouse C57BL6/J oocytes. We obtained 8 founder lines of which 2 (lines 4 and 15) showed strong expression in the vasculature throughout the entire body. The majority of the described imaging experiments were performed with animals derived from line 15. There is 13% mosaic expression of junctional eGFP::Claudin-5 protein within the adult CNS vasculature (both large vessels and capillaries; data not shown).

Mouse ischemic stroke model. All experimental procedures were approved by the IACUC committees at the University of California at Irvine, Stanford University and the Salk Institute for Biological Studies. 8- to 20-week-old male mice weighing 25-30 g were subjected to the transient filament occlusion (t-MCAO) model of ischemic stroke, as previously described (Arac et al., 2011). Mice were anesthetized with 1.5-2% isoflurane in 100% oxygen or a mixture of 20% oxygen and 80% air. The left external and common carotid arteries were permanently ligated and a 7-0 silicon rubber-coated, reusable monofilament (Docol Inc, 70SPRe2045) was inserted into the left common carotid artery and advanced towards the left internal carotid artery 9-10 mm after the left carotid bifurcation. The animal's core body temperature was maintained at 37°C throughout the surgery. Reperfusion was achieved by withdrawing the filament 45 minutes after the insertion.

After the closure of the surgical wound, the mice were returned to their cages with free access to water and food. *Cav1*^{-/-} males were obtained from the Jackson Laboratories (Bar Harbor, Maine).

Head plate implantation surgery for two-photon imaging. Adult *Tg eGFP-Claudin5* mice (8-20 weeks old) males were used for experiments. Surgery was done under isoflurane anesthesia (1-2%, mixed with 1–2 l/min O₂). Body temperature was kept at 37°C. For brain imaging, mice were implanted with a custom metal head plate, either on the day of imaging or up to five days before imaging as previously described (Nimmerjahn, 2012b). Hair, skin and periosteum overlying the neocortex were removed. After cleaning exposed skull areas, tissue adhesive (Vetbond, 3M) or cyanoacrylate glue (AccuTool Super Glue) and dental acrylic (H00335; Coltene Whaledent) were used to affix the head plate to the skull, keeping the intended imaging area uncovered. For one-time imaging, a craniotomy was performed (typically 1.3–2.0 mm in diameter and centered around -1.0 mm post-bregma and 3.5 mm lateral) leaving the *dura mater* intact (Nimmerjahn, 2012a). For repeated imaging over several days, a polished and reinforced thinned skull window was prepared ~24 h prior to imaging [typically 1.0-1.5 mm in diameter at -1.0 mm post-bregma and 3.5 mm lateral; reinforced with a #0 cover slip (Thomas Scientific) (Drew et al., 2010)]. For liver imaging, a laparotomy was performed and the liver was exteriorized. For muscle imaging, the dorsal part of a thigh muscle was exposed. In all one-time imaging experiments, the exposed tissue was covered with agar (1.5-2% type III-A, Sigma-Aldrich) in either PBS or artificial cerebral spinal fluid (ACSF) containing 125 mM NaCl, 5 mM KCl, 10 mM D-glucose, 10 mM HEPES, 2 mM CaCl₂ and 2 mM MgSO₄, (pH adjusted to 7.4 with NaOH) and a #1 cover slip (Thermo Fisher Scientific). To dampen heartbeat- and breathing-induced brain motion, a metal retaining ring was used to immobilize the cover slip.

***In vivo* two-photon imaging.** A custom upright two-photon microscope equipped with a pulsed femtosecond Ti:Sapphire laser (Chameleon Ultra II, Coherent or Tsunami, Spectra-Physics), two fluorescence detection channels and a water immersion objective (Olympus XLUMPlanFl 20X 0.95 numerical aperture (NA), Olympus LUMPLFLN 40X 0.8 NA, Zeiss W Achromplan 40X 0.8 NA, or Zeiss W Plan-Apochromat 63X 0.9 NA) was used for imaging. Blood plasma was labeled by tail vein injection (50-200 μ L) of biocytin-tetramethylrhodamine (TMR) or 3,000 MW dextran-TMR (1% in PBS). For simultaneous fluorescence excitation of GFP and TMR, 890-950 nm center wavelengths were used. Average laser powers used for imaging depended on tissue type, surgical preparation and imaging depth (typical values: <46 mW at \sim 300 μ m, <30 mW at \sim 80 μ m and <60 mW at \sim 350 μ m imaging depth for one-time brain, liver and muscle imaging, respectively; <37 mW at \sim 200 μ m for repeated transcranial imaging). Images were typically acquired at a 2 Hz frame rate using 512 x 512 pixel resolution and 4-frame averages. Image stacks contained up to 300 images and were typically acquired using 1 μ m axial spacing. Fields-of-view (FOVs) had a typical side length of 47-377 μ m. Repeated imaging of the same cortical volume over multiple days was achieved by precisely aligning the animal's head in a position determined during the first imaging session, using characteristic surface/intracortical blood vessels as reference structures (Nimmerjahn, 2012c). Head tilt was adjusted with \leq 0.5 degree precision using two orthogonally arranged collimated laser diodes (CPS180, Thorlabs) reflecting off the cover slip surface onto alignment targets (SM1A7, Thorlabs) and a dual axis goniometer (GN2, Thorlabs) with attached head plate holder. Image rotation was corrected online using MPScope image acquisition software (Nguyen et al., 2006). Lateral and axial image shifts in time-lapse recordings (e.g., due to t-MCAO-induced tissue swelling) were corrected offline in ImageJ by aligning images to reference

frames and creating image substacks based on reference stacks. ImageJ was also used to create overlay and maximum intensity projection images for quantitative image data analysis.

Following two-photon imaging experiments, animals were perfused with 4% paraformaldehyde in PBS, the brain was harvested and sectioned within 5.0 mm around the center of the imaging area (center coordinates: -1.0 mm post-bregma and 3.5 mm lateral; 1.0-2.0 mm diameter; 0-300 μ m depth). Coronal sections of brain tissue were stained for the tracer biocytin-TMR (see below) and Glut-1 to determine whether the area of imaging was within the stroke core region or penumbra. Animals were post-hoc classified as “stroke core-imaged animals” when the imaging area was clearly within the biocytin-TMR leakage area as outlined for example in Fig. 8A. Animals were post hoc classified as “stroke penumbra-imaged area” when the imaging area was either only partially within or immediately adjacent to the biocytin-TMR leakage area.

Immunofluorescence. Brains, muscles, livers and kidneys were harvested from wild-type C57BL6/J, *Tg eGFP-Claudin5*, *Caveolin1*^{-/-} or *Tg eGFP-Claudin5 Caveolin1*^{-/-} mice. For TJ protein immunofluorescence, tissues were fresh-frozen in TissueTek after perfusion with PBS. Tissue sections were fixed with 95% ethanol and acetone and stained for eGFP (1:1000; Life Technologies, CA), BSL-rhodamine (1:250; Vector laboratories, CA), ZO-1 (1:500; Life Technologies, CA) and Occludin (1:250; Life Technologies, CA) as described (Daneman et al., 2009). For other BBB or peripheral blood vessel markers, tissues were fixed for 6 hours with 4% PFA in PBS and cryoprotected in 30% sucrose before embedding in TissueTek. Sections were stained with antibodies for Caveolin1 (1:1000; Abcam, MA), Glut-1 (1:2000; EMD Millipore, MA), Collagen IV (1:1000; Abcam, MA), Nidogen (1:200; Millipore, CA) and Laminin-2 α (1:500; Abcam, MA) as well as BSL-FITC or BSL-rhodamine (1:250; Vector Laboratories, CA) (Daneman et al., 2009). Primary endothelial cells were labeled with alb-Alexa594 for 1 h as

described (Shajahan et al., 2004; Tirupathi et al., 2004), fixed with 4% PFA for 10 min at RT and stained with antibodies against EEA-1 (1:1000; Abcam, MA), LAMP-1 (1:400; Abcam, MA); Rab-4 (1:200; Abcam, MA), Rab-7 (1:100; Cell Signaling, MA), Caveolin1 (1:2000; Abcam, MA) and Caveolin2 (1:1000; Sigma, MO). Images were acquired with an LSM700 confocal microscope and processed with Fiji software.

Biocytin-TMR and IgG leakage quantitation. Brains and livers were harvested from 11-14 week-old C57BL6/J (Jackson Labs), *Tg eGFP-Claudin5* or *Caveolin1^{-/-}* mice (Jackson Labs) 30 - 45 min after tail vein injection with 1% biocytin-TMR (Invitrogen, CA). Tissues were then fixed with 4% paraformaldehyde in PBS overnight, and sectioned in 12 μ m-thick coronal slices with a Leica cryostat. Immunofluorescence was performed with antibodies for either Caveolin1 (1:1000; Abcam, MA) or Glut-1 (1:2000; EMD Millipore, MA) and FITC-conjugated *Griffonia (Bandeiraea) simplicifolia* lectin I (1:250; Vector Laboratories, CA). Streptavidin-Alexa594 (1:1000; Life Technologies, CA) was used to visualize biocytin-TMR distribution in tissues (Daneman et al., 2010) and Alexa488-conjugated mouse IgG (1:200) to visualize IgG leakage in the brain. Sections were imaged with an upright Zeiss Axioimager fluorescence microscope. Biocytin or IgG leakage was quantified with Fiji software. Brain slices were uniformly thresholded in order to quantify the total area of IgG or biocytin-TMR leakage. Areas that exceeded the threshold levels were defined as leakage area. Average intensity values for biocytin-TMR were gathered by selecting identical regions in ipsilateral or contralateral cortices or livers across subjects, then the ratio between the ipsilateral and contralateral cortex was determined.

Albumin leakage quantitation. Brains and livers were harvested from 11-14 week-old C57BL6/J mice (Jackson Labs), *Tg eGFP-Claudin5* mice or *Caveolin1^{-/-}* mice (Jackson Labs) subjected to t-

MCAO 30 min after tail vein injection of 1% albumin-Alexa594 (Life Technologies, CA). Tissues were fixed with 4% paraformaldehyde for 6 hours at 4°C, sectioned (12 µm coronal slices) with a Leica cryostat and then stained with fluorescent antibodies against Caveolin1 and Glut-1 (to visualize brain vasculature) or BSL-FITC (to visualize brain and liver vasculature). Sections were imaged with a LSM700 confocal microscope (Zeiss). The area of albumin present in endothelial cells or brain parenchyma was quantified using Fiji software. Glut-1 or BSL-I staining in cerebral blood vessels was automatically thresholded and separated from non-vasculature staining with the magic wand tool. Punctate albumin uptake in endothelial cells or brain parenchyma was then automatically thresholded. The vasculature area previously determined by Glut-1 or BSL-I staining was overlaid onto the albumin field of view in order to quantify endothelial cell-specific albumin endocytosis. The area of albumin endocytosis was calculated as percentage of blood vessel-associated albumin versus the total vasculature area in the image. The amount of albumin-Alexa594 not associated with blood vessels was used to determine the percentage of parenchyma-associated albumin that had transcytosed from the blood vessels into the tissues.

Statistical Analysis: For various analyses, we compared mean values among healthy controls versus *Tg eGFP-Claudin5* mice at various times post-t-MCAO (6-8 h, 12-14 h, 24-30 h and 48-58 h) using analysis of variance (ANOVA) models. We fitted a mixed-effect ANOVA model to account for potential correlation of multiple observations within the same mouse, and allowed comparisons between groups to be a fixed effect and random variations in measurements within the same mouse/animal to be a random effect. The only exceptions were Figures 4G and 5M,N where we ran a simple ANOVA model to compare mean values per mouse for various time points. For pairwise comparisons (Figures 6O,P and 8D), as well as comparisons of wild-type with *Tg eGFP-Claudin5* mice (Figure S2I-L), we fitted a mixed-effect model, where the pairwise

comparisons of two groups were indicated as fixed effects and the random variations in measurements within the same mouse/animal were accounted as random effects.

Transmission electron microscopy and immunoelectron microscopy. Samples from the ipsilateral or contralateral stroke cortex or healthy cortex were fixed in Karnovsky's fixative [2% glutaraldehyde (EMS Cat #16000) and 4% paraformaldehyde (EMS Cat #15700) in 0.1 M sodium cacodylate (EMS Cat #12300), pH 7.4] for 1 h at room temperature (RT) followed by overnight fixation at 4°C before they were processed for TEM. Samples were post-fixed in 1% osmium tetroxide (EMS Cat #19100) for 1 h at RT, washed 3X with water then stained *en bloc*, for either 2 h at RT or overnight at 4°C. Samples were then dehydrated in a series of ethanol washes (50%, 70%, 95% and 100%) for 15 min each at 4°C, followed by an acetonitrile wash for 15 min. Samples were then sequentially infiltrated with EMBED-812 resin (EMS Cat #14120) mixed 1:1 with acetonitrile for 2 h, followed by EMBED-812:acetonitrile (2:1) for 2 h. The samples were finally equilibrated into EMBED-812 for 2 h and placed into molds filled with gelatin capsules in a 65°C oven overnight. Sections between 75 and 90 nm were collected on a Leica Ultracut S (Leica, Wetzlar, Germany) and collected on formvar/carbon-coated slot grids (EMS Cat# FCF2010-Cu) or 100 mesh Cu grids (EMS Cat #FCF100-Cu). Grids were contrast stained for 15 min in 1:1 saturated uranyl acetate (~7.7%) to 100% ethanol, followed by staining in 0.2% lead citrate for 3 to 4 min. For immuno-EM, brains were fixed in 4% warm PFA for 6 h and sectioned with a cryostat. Sections were placed on polylysine-coated Thermanox plastic cover slips [Ted Pella Inc.; 26026 (22X60 mm)]. Brain sections were stained with anti-Caveolin-1 antibody overnight, followed by incubation with nanogold anti-rabbit IgG (1:50; Nanoprobes, Inc.) for 2 h at RT. The tissue was post-fixed with 4% PFA and 2% glutaraldehyde in 0.1 M sodium cacodylate at RT for 10 min. The gold particles were enhanced with the HQ SilverTM enhancement kit (Nanoprobes Inc.). Sections

were processed for TEM and imaged using a JEOL 1230 TEM at 80 kV. Photos were taken using a Gatan Orius digital camera. We obtained approximately 70 images of caveolae from randomly selected fields within the parietal cortex for each sample. The number of Cav1-positive vesicles visualized by immuno-EM were counted from each image and averaged for each sample.

TJ quantitation. We quantified the number of total TJs present and the fraction of TJs with gaps, protrusions or other abnormalities, in both two-photon and EM image data. For two-photon data we defined as one “eGFP⁺ TJ strand” a continuous junctional line between two endothelial cells without any bifurcation or interruption (see for example Figure 1C; yellow arrow). Note that in freeze-fracture EM data this eGFP⁺ line represents multiple TJ strands that form the TJs between two endothelial cells. To quantify TJ abnormalities in two-photon time-lapse data, we first created maximum intensity projections for each image stack/three-dimensional recording volume. In the resulting two-dimensional movies we then determined the number of protrusions, gaps and the fraction of dynamic protrusions and gaps for each time point. Blood vessel borders were defined using the biocytin-TMR or dextran-TMR costain (red fluorescence from these tracers delivered via the tail vein was simultaneously recorded with green fluorescence from eGFP-Claudin5). We quantified the total number of TJ strands in each projection and the fraction of TJs with gaps, protrusions or other abnormalities. Protrusions are identified as bulbous extensions from the otherwise linear TJ strands (see Figure 2K). Gaps are identified as TJ strand discontinuities of > 0.4 μm in length (see Figure 2K) for two-photon imaging data. The number of protrusions, gaps and the fraction of dynamic protrusions and gaps were determined for each time point of the time lapse series. To quantify TJ strands with abnormal morphology in EM data, we obtained approximately 70 images of TJs for each sample, counted the number of TJ strands that had

abnormalities (gaps in size ranging from 50-1000 nm; Figure 4C-F) for each image and calculated the percent of abnormal TJs (with gaps) versus total TJs.

Western blot analysis: Protein levels for BBB components in *Tg eGFP-Claudin5* versus wild-type mice or *Tg eGFP-Claudin5 Cav1^{-/-}* mice were assessed with the Odyssey Sa infrared imaging system (LI-COR, NE). Primary antibodies against Claudin5 (1:5000; Life Technologies, CA), Caveolin1 (1:10000; Abcam, MA), and Glut-1 (1:10000; EMD Millipore, MA) were used as BBB component markers, while β -actin (1:10000; Abcam, MA) was used as a protein control. IRDyes 680 and 800 (1:10000; LI-COR, NE) were used as secondary antibodies. Protein values were quantitated using Odyssey imaging software. Levels of Claudin5, Glut-1 or Caveolin1 proteins in *Tg eGFP-Claudin5* mice are presented as a percentage of the identical protein levels in wild-type mice, with each being normalized to its respective β -actin control value.

Flow cytometry analysis of the hematopoietic system in *Tg eGFP-Claudin5* mice. Blood was collected through cardiac puncture in EDTA-containing syringes and the spleen, axillary lymph nodes and tibia bones were harvested. The spleen and lymph nodes were passed through a 40 μ m cell strainer for homogenization and bone marrow was flushed from the bones. Red blood cells in all organs were lysed with lysis buffer (7.47 g ammonium chloride and 2.04 g Tris base in 1 L ddH₂O, pH 7.6), and cells were washed with 10% FBS in DMEM and kept on ice until staining. The cells were first stained with 0.1% Live/Dead-Aqua (Life Technologies, CA) to exclude dead cells from the analysis, then blocked with 1% anti-mouse CD16/32 (eBioscience, CA) antibody and 10% mouse serum (Jackson ImmunoLab, PA) in MRB buffer [5% bovine serum albumin (Sigma, MO) and 2 mM EDTA in PBS]. Cells were incubated with following antibodies for 20

min at 4°C: anti-mouse CD45 (30-F11), CD11b (M1/70), CD11c (N418), CD3e (17A2), CD8b (eBioH35-17.2), B220 (RA3-6B2) (eBioScience, CA) and CD4 (RM4-5; Life Technologies, CA). Flow cytometry was performed on a Becton Dickinson LSR-II (Stanford shared FACS facility), and data were analyzed using FlowJo (TreeStar Inc). Gates were set based on the unstained cells, and compensation was achieved by single-color, stained BD-CompBeads (BD Biosciences, CA).

Supplemental References

Arac, A., Brownell, S.E., Rothbard, J.B., Chen, C., Ko, R.M., Pereira, M.P., Albers, G.W., Steinman, L., and Steinberg, G.K. (2011). Systemic augmentation of alphaB-crystallin provides therapeutic benefit twelve hours post-stroke onset via immune modulation. *Proceedings of the National Academy of Sciences of the United States of America* *108*, 13287-13292.

Daneman, R., Agalliu, D., Zhou, L., Kuhnert, F., Kuo, C.J., and Barres, B.A. (2009). Wnt/beta-catenin signaling is required for CNS, but not non-CNS, angiogenesis. *Proceedings of the National Academy of Sciences of the United States of America* *106*, 641-646.

Daneman, R., Zhou, L., Kebede, A.A., and Barres, B.A. (2010). Pericytes are required for blood-brain barrier integrity during embryogenesis. *Nature* *468*, 562-566.

Drew, P.J., Shih, A.Y., Driscoll, J.D., Knutsen, P.M., Blinder, P., Davalos, D., Akassoglou, K., Tsai, P.S., and Kleinfeld, D. (2010). Chronic optical access through a polished and reinforced thinned skull. *Nat. Methods* *7*, 981-984.

Evans, V., Hatzopoulos, A., Aird, W.C., Rayburn, H.B., Rosenberg, R.D., and Kuivenhoven, J.A. (2000). Targeting the Hprt locus in mice reveals differential regulation of Tie2 gene expression in the endothelium. *Physiol Genomics* *2*, 67-75.

Nguyen, Q.T., Tsai, P.S., and Kleinfeld, D. (2006). MPscope: a versatile software suite for multiphoton microscopy. *J. Neurosci. Methods* *156*, 351-359.

Nimmerjahn, A. (2012a). Optical window preparation for two-photon imaging of microglia in mice. *Cold Spring Harb. Protoc.* *2012*, 587-593.

Nimmerjahn, A. (2012b). Surgical implantation of a head plate in mice in preparation for in vivo two-photon imaging of microglia. *Cold Spring Harb. Protoc.* *2012*, 583-586.

Nimmerjahn, A. (2012c). Two-photon imaging of microglia in the mouse cortex in vivo. *Cold Spring Harb. Protoc.* *2012*, 594-603.

Schlaeger, T.M., Bartunkova, S., Lawitts, J.A., Teichmann, G., Risau, W., Deutsch, U., and Sato, T.N. (1997). Uniform vascular-endothelial-cell-specific gene expression in both embryonic and adult transgenic mice. *Proc Natl Acad Sci USA* *94*, 3058-3063.

Shajahan, A.N., Tirupathi, C., Smrcka, A.V., Malik, A.B., and Minshall, R.D. (2004). Gbetagamma activation of Src induces caveolae-mediated endocytosis in endothelial cells. *J Biol Chem* *279*, 48055-48062.

Tirupathi, C., Naqvi, T., Wu, Y., Vogel, S.M., Minshall, R.D., and Malik, A.B. (2004). Albumin mediates the transcytosis of myeloperoxidase by means of caveolae in endothelial cells. *Proc Natl Acad Sci USA* *101*, 7699-7704.